Supporting Information

Improving ionic conductivity of polymer electrolytes induced by ceramic nanowire fillers with abundant lithium vacancies

Jianlong Ding, Wenqiang Wang*, Yifan Zhang, Hongchun Mu, Xiaomin Cai, Zhengyu Chang, Gengchao Wang*

Experimental Section

Preparation of S/C composite cathodes

Sulfur powder and polyacrylonitrile-based carbon fiber were milled in agate mortar with a mass ratio of 1:3. The cathode materials were obtained by melting in an argon atmosphere at 155 °C for 12 h. The electrode was prepared by ball milling the cathode materials, acetylene black, and PVDF binder in a mass ratio of 8:1:1 for 4 h. The obtained slurry was coated on the aluminum foil and dried for 12 h at 50 °C in a vacuum oven.

Density functional theory (DFT)-based calculations

The generalized gradient approximation (GGA) electronic calculations were performed using the Vienna Ab initio Simulation Package (VASP). For DFT calculations, projector augmented-wave (PAW) potentials for Li, La, Al, Zr, Ta, and O atoms, plane-wave basis set with a cutoff of 500 eV, and Perdew–Burke–Ernzerh (PBE) of GGA functionals were used. The crystal parameters, refined through XRD data, served as the initial parameters for DFT structural optimizations.

Bond Valence Site Energy (BVSE) calculations were performed to investigate the Li-ion migration path and energy barriers with the softBV program. The structural models were obtained from the DFT structural optimization. The energies of the different Li sites in the crystal structure were calculated against a 3D grid of points with 0.1 Å resolution using the transferable Morse-type softBV force field. The crystal structure and ionic migration path were visualized using the VESTA software.

Results and discussion

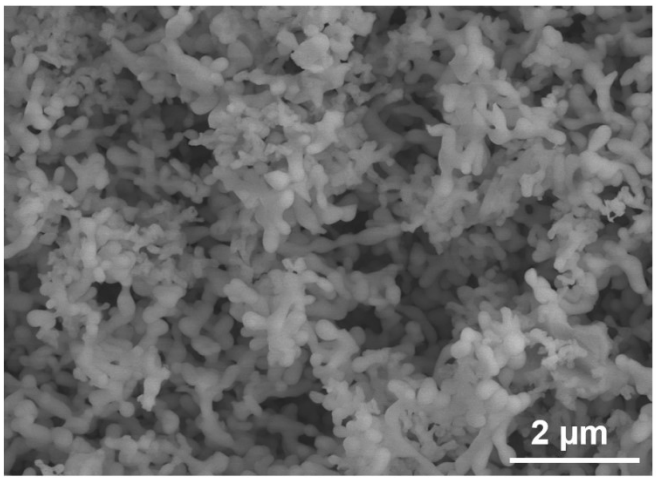

Figure S1. FESEM image of TALLZO NWs by one-step sintering.

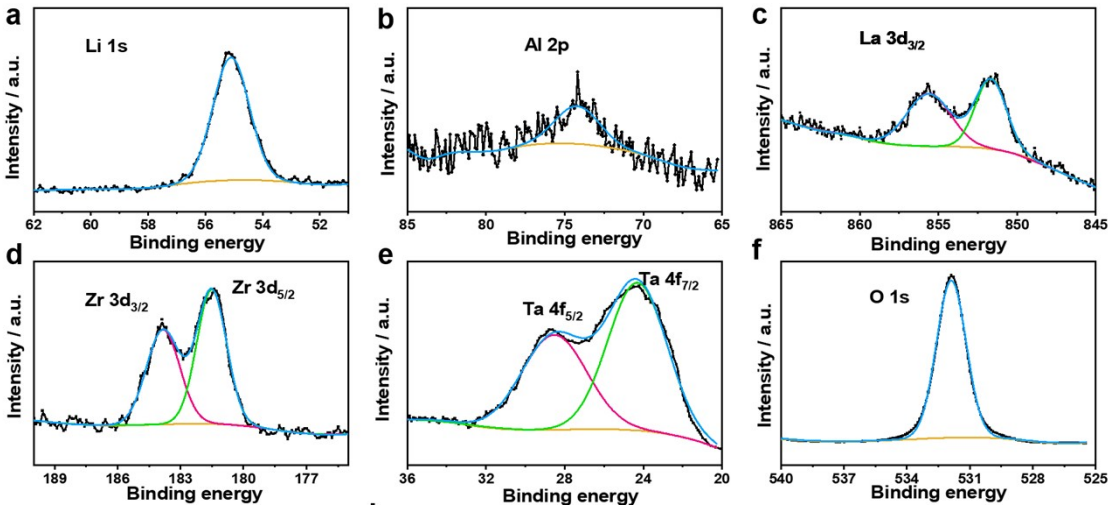

Figure S2. XPS spectra of the TALLZO including (a) Li *1s*, (b) Al *2p*, (c) La *3d*, (d) Zr *3d*, (e) Ta *4f*, (f) O *1s*.

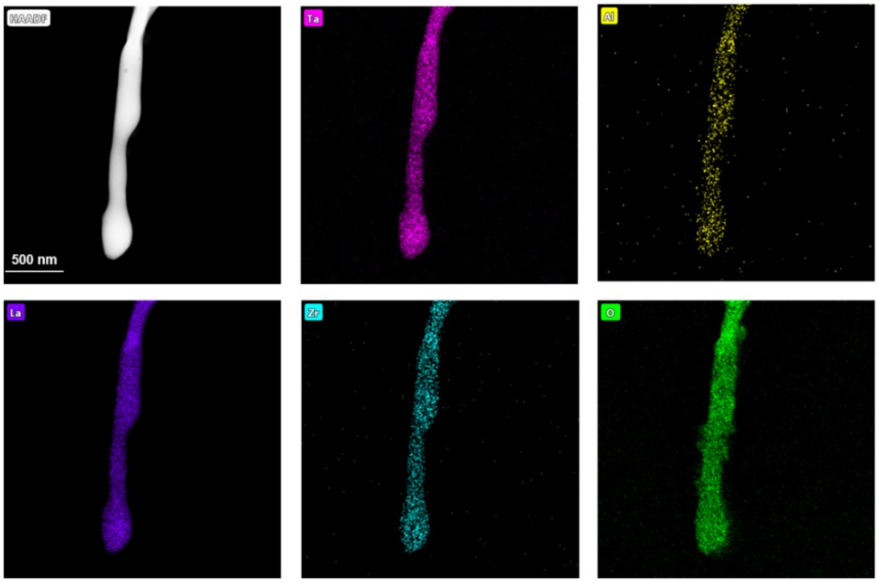

Figure S3. HAADF-STEM image and corresponding elemental mappings of TALLZO NWs.

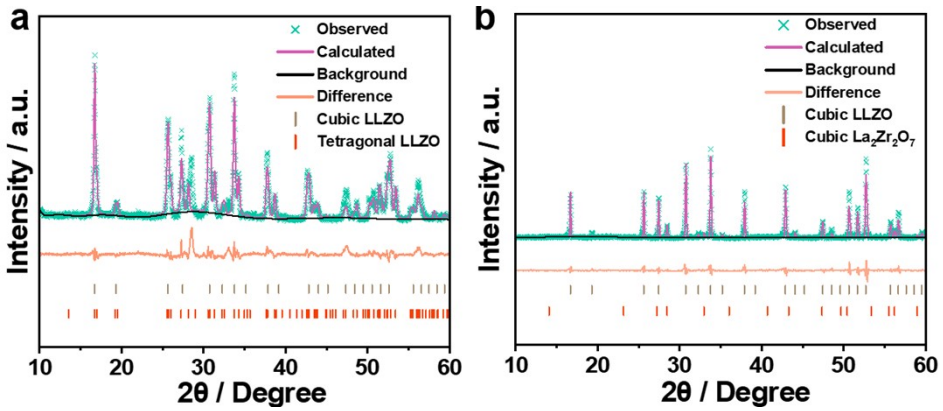

Figure S4. Rietveld refined the XRD results of LLZO and ALLZO NWs.

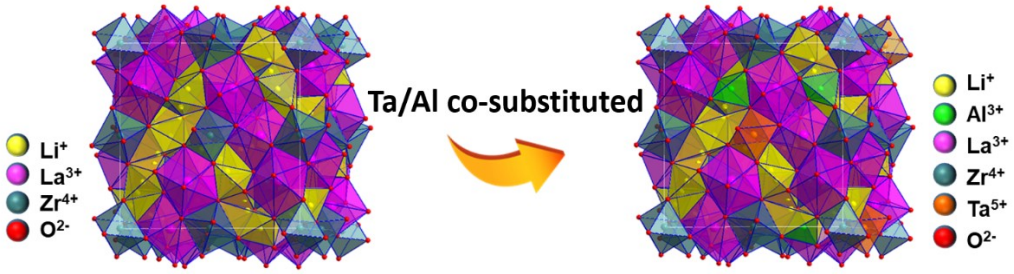

Figure S5. The cubic structure of garnet LLZO and the position substituted by Ta^{5+} and Al^{3+}.

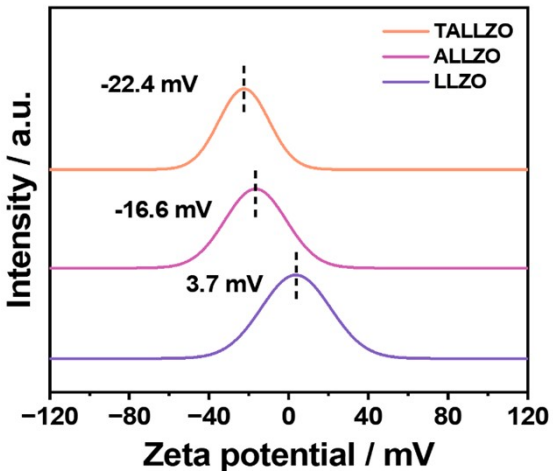

Figure S6. Zeta potential of LLZO, ALLZO and TALLZO

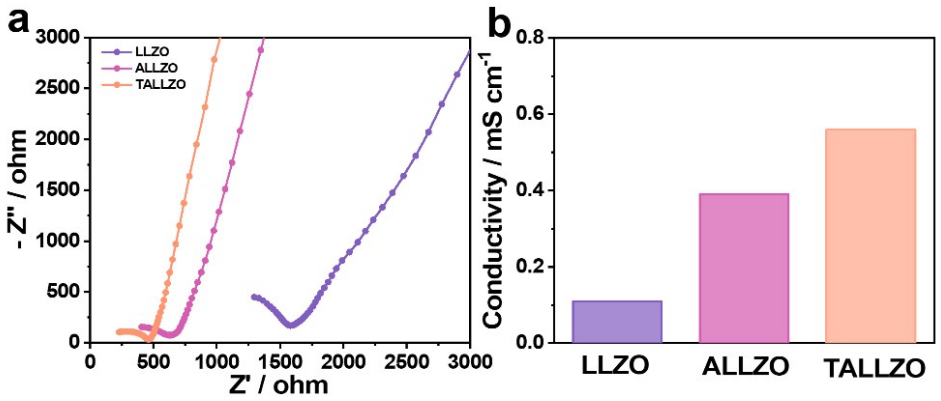

Figure S7. (a) EIS spectra and (b) Ionic conductivity of LLZO, ALLZO, and TALLZO.

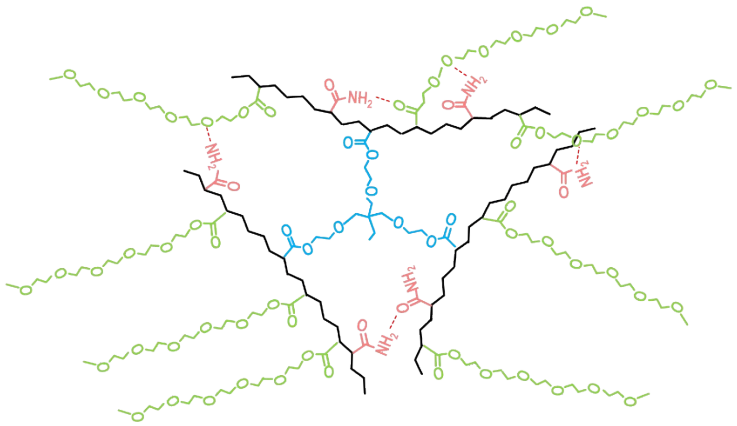

Figure S8. Schematic diagram of structure for the P-E-A comb polymer network.

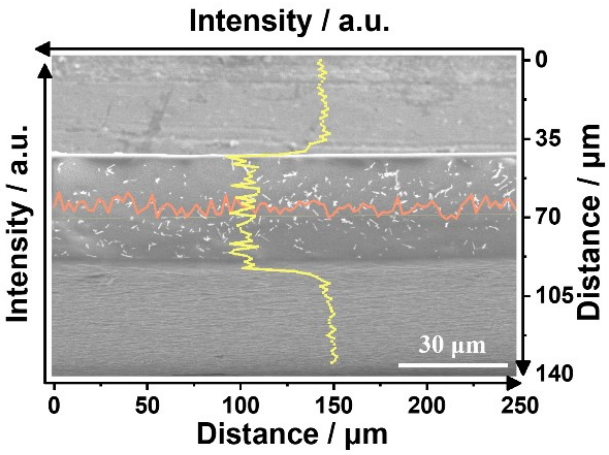

Figure S9. Side-view SEM image and EDS Zr elemental linear scanning of the P-E-A@TALLZO NWs CPE.

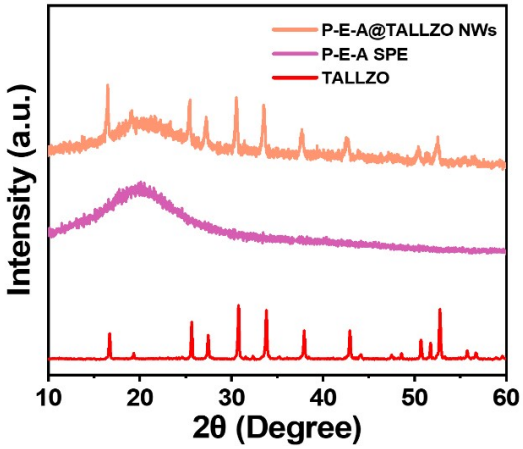

Figure S10. XRD patterns of the TALLZO, P-E-A SPE, and P-E-A@TALLZO NWs CPE.

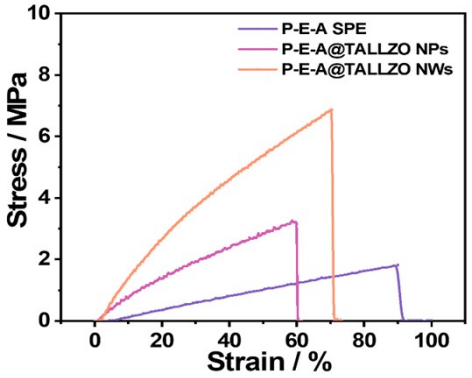

Figure S11. Stress-strain curves of P-E-A SPE, P-E-A@TALLZO NPs CPE, and P-E-A@TALLZO NWs CPE.

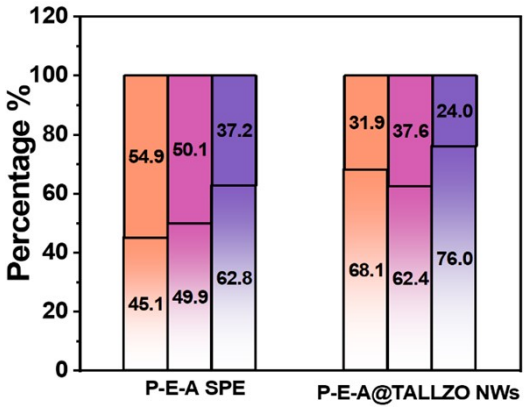

Figure S12. The percentages of integral areas calculated from the fitted FT-IR spectra of Fig. 3a, b.

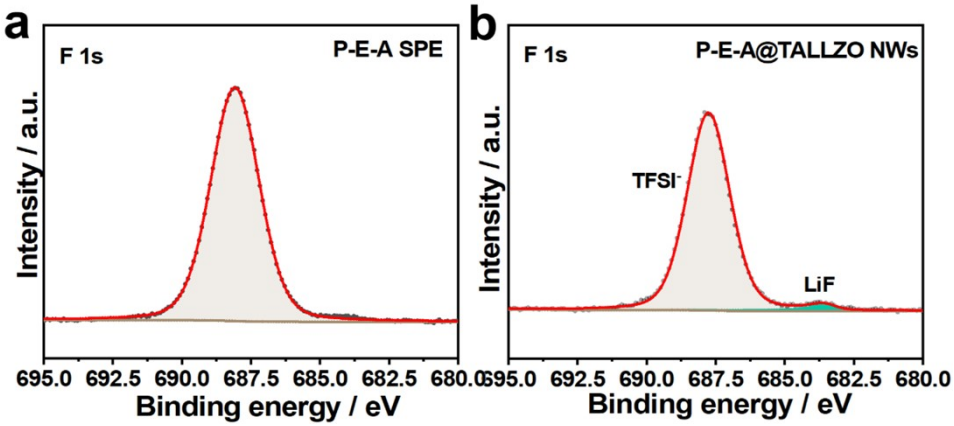

Figure S13. The XPS F1s spectra of (g) P-E-A SPE and (h) P-E-A@TALLZO NWs CPE.

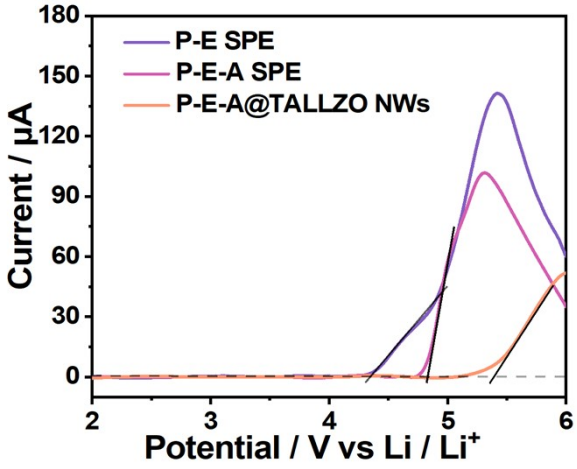

Figure S14. LSV profiles of SS//P-E SPE//Li, SS//P-E-A SPE//Li, and SS//P-E-A@TALLZO NWs CPE//Li.

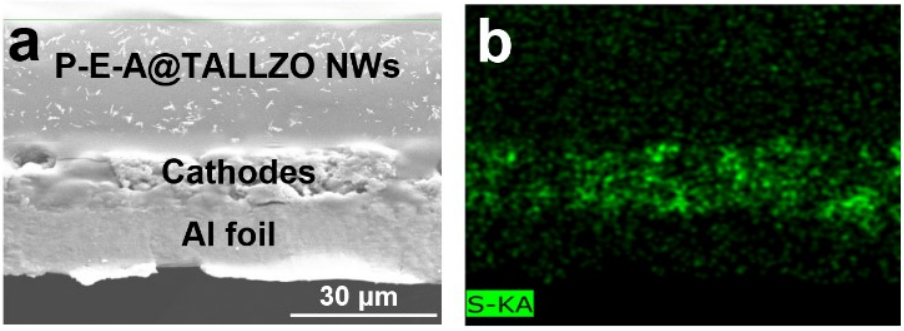

Figure S15. Side-view SEM image and corresponding S elemental mappings of integrated cathode-electrolyte structure.

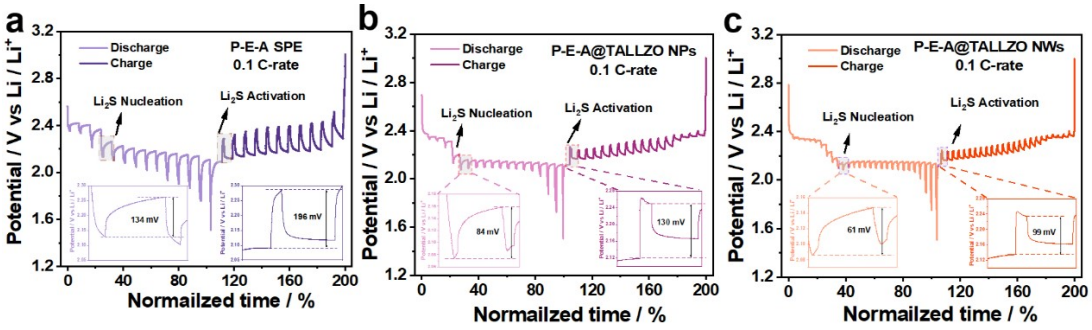

Figure S16. GITT profiles of ASSLSBs for (a) P-E-A SPE, (b) P-E-A@TALLZO NPs CPE, and (c) P-E-A@TALLZO NWs CPE.

Table S1. Property comparison of the PEO-based solid polymer electrolytes with previously reported research.

Electrolytes/ Battery system	Filler content (wt%)	Ionic conductivity (S cm^{-1})	Li^+ transfer number	Battery performance (specific capacity / mAh g^{-1})	Ref.
PEO/LiTFSI Li-S cell	LLTO NWs (13 wt%)	2.3×10^{-4} (25°C)	——	415 mAh g^{-1}(50th cycle) (0.05 C, 25°C)	[7]
PEO/SN/LiTFSI $LiFePO_4$/Li cell	Nb/Al-LLZO NPs (10 wt%)	3.09×10^{-4} (25 °C)	0.75	152.3 mAh g^{-1}(1st cycle) vs. 137 mAh g^{-1}(200th cycle) (0.2 C, 45°C)	[41]
PVDF/LiTFSI $LiFePO_4$/Li cell	Al-LLZO NWs (15 wt%)	1.712×10^{-4} (25°C)	0.72	166 mAh g^{-1}(1st cycle) vs. 159 mAh g^{-1}(120th cycle) (0.1 C, 25°C)	[42]
PEO/LiTFSI $LiFePO_4$/Li cell	NH_4F-LLZO NPs (7.5 wt%)	1.28×10^{-3} (60°C)	0.33	136 mAh g^{-1}(1st cycle) vs. 123 mAh g^{-1}(300th cycle) (2 C, 60°C)	[43]

PPC/PET/LiTFSI $LiFePO_4$/Li cell	LLZTO@PDA NPs (5 vol%)	3.2×10^{-4} (30°C)	0.69	126 mAh g^{-1}(1st cycle) vs. 124 mAh g^{-1}(50th cycle) (0.1 C, 30°C)	[44]
PEO- LiTFSI NCM811/Li cell	$Gd_{0.1}Ce_{0.9}O_{1.95}$ NPs (5 wt%)	1.9×10^{-4} (30°C)	0.26	135 mAh g^{-1}(1st cycle) vs. 100 mAh g^{-1}(100th cycle) (100 μA cm^{-2}, 35°C)	[45]
PEO/LiTFSI $LiFePO_4$/Li cell	LLZO@WO_3 NPs (10 wt%)	1.9×10^{-4} (40°C)	0.67	159.2 mAh g^{-1}(1st cycle) vs. 144.3 mAh g^{-1}(400th cycle) (1 C, 40°C)	[46]
PEO/PVDF/LiTFSI NCM811/Li cell	Gd-CeO_2 NWs (11 wt%)	2.3×10^{-4} (30°C)	0.64	126.3 mAh g^{-1}(1st cycle) vs. 95.4 mAh g^{-1}(250th cycle) (0.5 C, 50°C)	[47]
P-E-A/LiTFSI Li-S cell	Ta/Al-LLZO NWs (10 wt%)	3.80×10^{-4} (25°C)	0.79	776 mAh g^{-1} (1st cycle) vs. 634 mAh g^{-1}(200th cycle) (0.1 C, 25°C)	This work